


## Alternative explanation for the relaxor ferroelectric behavior in FeTiNbO<sub>6</sub> rutile ceramics: The influence of electrode contacts

Thomas E. Hooper<sup>✉,\*</sup>, Tsz Kin Chan, and Derek C. Sinclair<sup>✉,†</sup>

*Department of Materials Science and Engineering, Sir Robert Hadfield Building, University of Sheffield, Mappin Street, Sheffield S1 3JD, United Kingdom*

 (Received 9 August 2023; revised 28 September 2023; accepted 4 October 2023; published 2 November 2023)

The radio-frequency permittivity-temperature profiles of acceptor-donor codoped TiO<sub>2</sub>-based rutiles commonly produce higher than expected values ( $>10^3$  at 300 K) often with conflicting interpretations. A combination of dielectric spectroscopy (DS) and impedance spectroscopy (IS) with different electrode materials is used to reinvestigate the electrical properties of Fe<sup>3+</sup>-Nb<sup>5+</sup>-doped rutile in the form of FeTiNbO<sub>6</sub> ceramics that show permittivity-temperature characteristics that are consistent with relaxor ferroelectrics (RFE). IS results reveal semiconducting grains with an activation energy of  $\sim 0.16$  eV, and relative permittivity of similar magnitude and temperature dependence to undoped TiO<sub>2</sub> ( $<250$ ). Reducing the work function of the electrode material by replacing Au with InGa has a dramatic effect on the IS and DS data. We propose the apparent RFE behavior observed by DS and previously attributed to the formation of nanoclustering of the cations is an extrinsic effect primarily associated with the development of Schottky barriers between the semiconducting ceramics and Au contacts.

DOI: [10.1103/PhysRevMaterials.7.114401](https://doi.org/10.1103/PhysRevMaterials.7.114401)

### I. INTRODUCTION

The defect chemistry of undoped TiO<sub>2±x</sub> in the form of rutile single crystals and polycrystalline ceramics has been widely explored for a range of functionality [1–4]. The precise composition controls the electrical properties and is highly dependent on the preparation conditions (temperature-time-*p*O<sub>2</sub>) and can exhibit *n*-type ( $x < 0$ ), intrinsic ( $x = 0$ ), and *p*-type ( $x > 0$ ) behavior [3]. Stoichiometric ( $x = 0$ ) TiO<sub>2</sub> is a wide band-gap insulator that exhibits incipient ferroelectric behavior where the permittivity rises on cooling from  $\sim 170$  at room temperature to  $\sim 257$  at  $\sim 50$  K, where it then plateaus to  $\sim 4$  K [5–7]. There is no appreciable frequency dependence of the permittivity over the kHz to MHz range and the permittivity data can be fitted to the Barrett equation, which is a modified form of the Curie-Weiss law [8]. The higher than expected permittivity behavior is attributed to a combination of the high polarizability and second-order Jahn-Teller distortions associated with the Ti<sup>4+</sup> (*d*<sup>0</sup>) ions.

A large range of mid-sized cations can be doped into TiO<sub>2</sub> to form a range of nominally stoichiometric di- and trirutiles, *MM'*O<sub>4</sub> and *MM''M''*O<sub>6</sub>, respectively [9]. In the case of trirutiles, many are based on a combination of acceptor-donor pairs, for example Fe<sup>3+</sup>-Ta<sup>5+</sup> in FeTiTaO<sub>6</sub>, Fe<sup>3+</sup>-Nb<sup>5+</sup> in FeTiNbO<sub>6</sub>, and Cr<sup>3+</sup>-Sb<sup>5+</sup> in CrTiSbO<sub>6</sub>. In several cases,

there have been reports of high permittivity values ( $>10^3$ ) and relaxor ferroelectric (RFE) behavior at elevated temperatures ( $>500$  K) despite the lack of any evidence of structural phase transitions and/or justifications based on noncentrosymmetric space groups. Instead, the RFE behavior has been attributed to the formation of polar nanodomains associated with clustering of the various cations [10,11]. It has been reported that Fe<sup>3+</sup> containing Nb<sup>5+</sup>, Ta<sup>5+</sup>, and Sb<sup>5+</sup> trirutiles such as FeTiNbO<sub>6</sub>, FeTiTaO<sub>6</sub>, and FeTiSbO<sub>6</sub> are susceptible to these large permittivities [10–12] that are comparable to the best relaxor materials like Pb(Mg<sub>1/3</sub>Nb<sub>2/3</sub>)O<sub>3</sub> [13,14]. However, Ga<sup>3+</sup> and Al<sup>3+</sup> analogs do not show this type of behavior and have room-temperature permittivity values  $<50$  [11], which is consistent with that expected for doped rutiles that contain less polarizable ions than Ti<sup>4+</sup>.

Low acceptor-donor In<sup>3+</sup>-Nb<sup>5+</sup> and Ga<sup>3+</sup>-Nb<sup>5+</sup> levels in [(Ga or In)<sub>0.5</sub>Nb<sub>0.5</sub>]<sub>x</sub>Ti<sub>1-x</sub>O<sub>2</sub> for  $x = 0.005$  to 0.10 have attracted much attention in the last decade as so-called colossal permittivity (CP) materials [15–25]. In contrast to temperature-dependent RFE behavior, they exhibit large temperature- and frequency-independent permittivity ( $>10^4$ ) with low dielectric loss ( $<0.1$ ) over a wide temperature range from  $\sim 50$  to 450 K. This behavior was initially attributed to the development of electron-pinned defect dipoles at low dopant levels [17,18,20]. However, many subsequent studies on single crystals and ceramics based on dielectric spectroscopy or impedance spectroscopy have shown this CP to be related to grain boundary and/or surface layer-electrode contact Maxwell-Wagner effects based on *n*-type semiconducting bulk (grains) and insulating grain boundaries/surface layers/nonohmic electrode contacts [15,16,19,21–25]. The mechanisms and CP behavior are therefore very similar to that observed in *n*-type CaCu<sub>3</sub>Ti<sub>4</sub>O<sub>12</sub> [26–28] and can be

\*Corresponding author: [t.e.hooper@sheffield.ac.uk](mailto:t.e.hooper@sheffield.ac.uk)

†Corresponding author: [d.c.sinclair@sheffield.ac.uk](mailto:d.c.sinclair@sheffield.ac.uk)

attributed to a combination of surface and/or internal barrier-layer capacitance mechanisms.

Recently, it has been shown that it is challenging to control the precise acceptor-donor stoichiometry at these low doping levels ( $x \leq 0.1$ ) in  $\text{TiO}_2$  crystals [19,24]. During processing, low levels of nonstoichiometry associated with the Nb-acceptor ratio (primarily loss of In and Ga) occur and the excess of donors gives rise to delocalized electrons (in the bulk) that result in high dielectric losses with the development of Schottky barriers at the electrodes that gives rise to permittivity  $>10^4$ . Adjusting the stoichiometry by annealing samples in sacrificial powder of the acceptor material (i.e.,  $\text{In}_2\text{O}_3$  or  $\text{Ga}_2\text{O}_3$ ) dramatically reduces the permittivity and the dielectric losses to values and behavior more akin to undoped  $\text{TiO}_2$  [19,24]. Low levels of acceptor-donor nonstoichiometry therefore appear to be crucial for simultaneously obtaining the CP behavior with permittivity  $>10^4$  and low dielectric loss.

The electrical properties of nominally stoichiometric trirutiles (where  $x = 0.67$ ) such as  $\text{FeTiTaO}_6$  and  $\text{FeTiNbO}_6$  have primarily been studied at and above room temperature (RT) via dielectric spectroscopy (DS), which is based on variable-temperature, fixed-frequency real and imaginary components of permittivity [10–12]. At present, all these compounds have been considered to be stoichiometric and fixed valence with respect to each cation present and the permittivity data of interest therefore assumed to be associated with insulating (dielectric) materials. This valency assumption is reasonable for acceptor-dopants such as Ga and Al ( $p$ -block elements) with a fixed oxidation state of +III; however, transition-metal “acceptors” can exhibit variable oxidation states, e.g., +II, +III, and +IV in the case of Fe. If these dopants exhibit mixed oxidation states in these compounds they can potentially give rise to appreciable levels of electronic conduction and space-charge effects and therefore be a contributing source to the reported high-permittivity values [10–12].

Impedance spectroscopy (IS) is a versatile technique to probe the electrical properties of single crystals and/or ceramics as it can facilitate grain, grain-boundary, and electrode effects to be identified at various temperatures and frequencies based on their respective time constants. Analyzing IS data based on an appropriate equivalent circuit permits the resistance ( $R$ ) and capacitance ( $C$ ) values for the different electroactive regions to be obtained and their temperature dependencies to be established. IS data are often presented in literature as the imaginary component  $Z''$  against real  $Z'$  which form a semicircle (or semicircles) representing a single (or multiple)  $RC$  element(s). However, in cases of electrical heterogeneity, the region of highest resistance may be localized (such as a grain boundary) and dominate the impedance plot. In cases like these, it is useful to plot the electrical modulus,  $M^*$ , as shown in Eq. (1):

$$M^* = j\omega C_0 Z^*, \quad (1)$$

where  $\epsilon_0$  is the permittivity of free space,  $A$  is the electrode area, and  $l$  is the electrode separation, where  $j = \sqrt{-1}$ ,  $\omega$  is angular frequency  $= 2\pi f$ ,  $C_0 = \epsilon_0 A/l$  and  $Z^*$  is the complex impedance.  $M^*$  and  $Z^*$  are intrinsically weighted to probe different regions of the electrical microstructure, highlighting the most resistive and least capacitive elements, respectively,

with the higher-frequency  $M''$  peak representing the bulk component of the material [29]. Here, we present IS and DS data for  $\text{FeTiNbO}_6$  ceramics from 10 to 650 K. A combination of  $Z^*$  plots and  $Z''$  and  $M''$  spectra are used to deconvolute the intrinsic (bulk) and extrinsic (grain boundaries, surface layers, and/or electrode effects) contributions to polarization and demonstrated the presence of electrical heterogeneity in these ceramics. A semiconducting grain response can be accessed using  $M^*$  plots/ $M''$  spectra below 300 K over the accessible range of  $\sim 10$ – $10^6$  Hz. The magnitude and temperature dependence of the bulk permittivity are comparable to undoped  $\text{TiO}_2$  and the activation energy for the semiconductivity is  $\sim 0.16$  eV. From RT and above, the resistive regions that are extrinsic in nature, e.g., grain boundaries, surface layers, and/or electrode effects are accessed by  $Z^*$  plots/ $Z''$  spectra and by changing the electrode material. We propose these extrinsic contributions are responsible for the large permittivity values observed in DS data in the region of 500–650 K as opposed to any intrinsic RFE behavior.

## II. EXPERIMENT

Commercially available reagent powders of  $\text{Fe}_2\text{O}_3$  (99%, Sigma-Aldrich),  $\text{TiO}_2$  (99.9%, Sigma-Aldrich), and  $\text{Nb}_2\text{O}_5$  (99.5%) were dried for 8 h ( $\text{Fe}_2\text{O}_3$  at 600 °C,  $\text{Nb}_2\text{O}_5/\text{TiO}_2$  at 900 °C) in a muffle furnace before weighing in stoichiometric quantities to form  $\text{FeTiNbO}_6$ . Powders were ground in isopropanol using an agate pestle and mortar for 30 min, placed into an alumina crucible, and calcined at 1300 °C for 6 h in air. Reacted powders were ground again for 30 min in isopropanol using an agate pestle and mortar, uniaxially pressed at 12.5 MPa into 10-mm pellets, and sintered at 1325 °C for 5 h.

X-ray diffraction (XRD) was carried out using a PANalytical Aeris diffractometer (Malvern Panalytical Ltd, UK) on crushed, sintered pellets annealed at 600 °C for 1 h (cooling rate of 50 °C/h) using a Cu radiation source, a step size of 0.02°, and voltage and current of 30 kV and 40 mA, respectively. Ceramic microstructure was analyzed using an Inspect F SEM (scanning electron microscope, FEI, Netherlands) with an accelerating voltage of 20 kV and working distance of 10.6 mm. Samples were polished beforehand using diamond paste (Beuhler) from 6 to 1  $\mu\text{m}$  and thermally etched at 1125 °C for 15 min before sputter coating a 5-nm Au layer to avoid charging. For electrical measurements, samples were ground and polished using SiC paper and electroded using fire-on Au paste at 850 °C for 2 h. High-temperature DS and IS analysis was carried out using an Agilent E4980A Precision LCR Meter connected to a tube furnace. Subambient DS and IS analysis was carried out using an Agilent E4980A Precision LCR Meter connected to a Cryodrive 1.5 cryocooler (Oxford Instruments, UK). IS measurements were carried out using a 0.1 V AC signal from 20 Hz to 1 MHz at 25 °C intervals with 20-min waiting time to thermally equilibrate the sample.

## III. RESULTS AND DISCUSSION

All reflections in the XRD patterns for sintered ceramics of  $\text{FeTiNbO}_6$  were indexed on space group  $P4_2/mnm$  with  $a = 4.6574(63)$  and  $c = 3.0156(22)$  Å (Supplemental

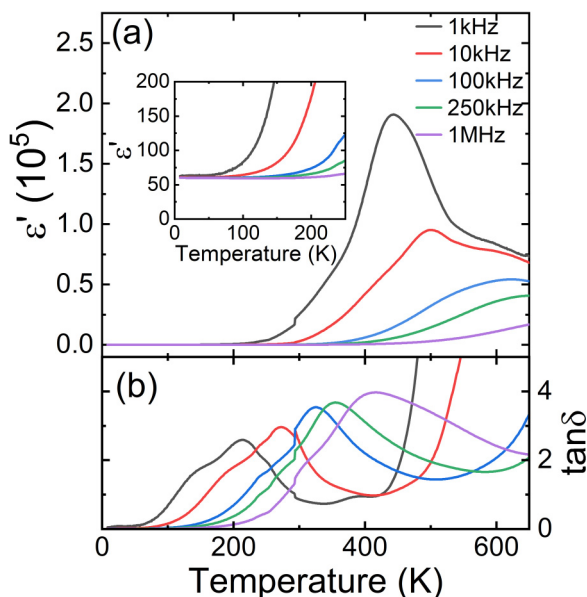


FIG. 1. (a) Permittivity and (b)  $\tan \delta$  vs temperature for FeTiNbO<sub>6</sub> ceramics. Discontinuities are where high temperature and subambient DS datasets have been stitched.

Material Fig. S1 [30]) and confirm the ceramics to be single phase. Geometric density was estimated to be  $\sim 93\%$  of the theoretical density based on unit-cell volume from the measured lattice parameters. SEM images confirmed the density measurements and the microstructure consisted of grains with an average grain size of  $36 \mu\text{m}$  (Supplemental Material, Fig. S2).

The DS data from  $\sim 10$  to  $650$  K are shown in Fig. 1.  $\epsilon'$  at  $\sim 10$  K is  $\sim 60$  and shows little frequency dependence; however, it begins to rise rapidly above  $\sim 50$  K and shows strong frequency dependence [Fig. 1(a), inset]. There is a clear maximum in  $\epsilon'$  between  $400$  and  $650$  K for the  $1$  kHz ( $\epsilon'_{\text{max}} \sim 200000$ ) to  $100$  kHz data ( $\epsilon'_{\text{max}} \sim 50000$ ) with  $T_{\text{max}}$  increasing with frequency. There is also evidence of a shoulder with  $\epsilon' \sim 75000$  at  $\sim 600$  K for the  $1$  and  $10$  kHz datasets. For the  $250$  kHz and  $1$  MHz datasets  $\epsilon'$  increases with temperature but no peak(s) are observed within the measured temperature range. The RT to  $600$  K permittivity data are consistent with a previous DS study of FeTiNbO<sub>6</sub> ceramics; however, no subambient DS data were reported [11].

There are multiple peaks observed in the  $\tan \delta$  datasets [Fig. 1(b)], and  $\tan \delta_{\text{max}}$  all occur at much lower temperatures ( $< 400$  K) than those obtained from their respective  $\epsilon'$  data. The magnitude and temperature associated with the  $\tan \delta_{\text{max}}$  peak increase with increasing frequency from  $\sim 2.5$  at  $\sim 200$  K for  $1$  kHz to  $\sim 4$  at  $400$  K for  $1$  MHz. It is also notable that  $\tan \delta$  data show additional features with clear evidence of a thermally activated shoulder below  $\tan \delta_{\text{max}}$  for all frequencies and a higher-frequency shoulder and an additional (smaller) peak at  $\sim 400$  K for the  $1$  kHz data. With the exception of the  $1$  MHz dataset,  $\tan \delta$  rises steeply at temperatures beyond the peak in  $\tan \delta$ , which is indicative of space-charge polarization [31].

Complex impedance plane,  $Z^*$ , plots at  $300$  K showed the response of ceramics with Au electrodes to be

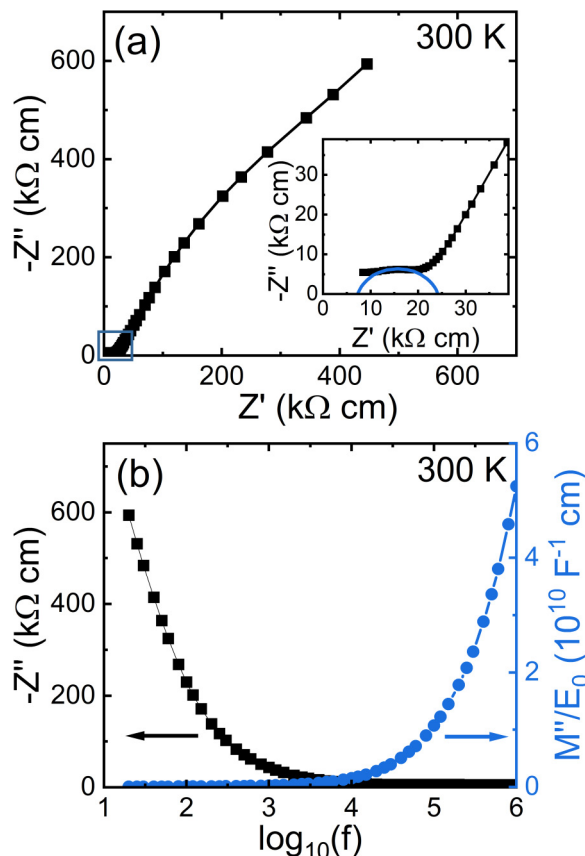


FIG. 2. (a)  $Z^*$  plot and (b)  $Z''$  and  $M''$  spectra for FeTiNbO<sub>6</sub> ceramics at  $300$  K. Inset in (a) shows  $Z^*$  plot on expanded scale close to the origin.

electrically heterogeneous, containing both semiconducting and insulating components. To a first approximation, the IS data could be modeled on (at least) three parallel  $RC$  elements connected in series: bulk, surface layer, and nonohmic electrode contacts, as justified below. The inset in Fig. 2(a) shows evidence of a high-frequency, nonzero intercept on the  $Z'$  axis at  $\sim 10$  k $\Omega$  cm, followed by a small intermediate-frequency arc with an associated  $R$  and  $C$  of  $\sim 12.5$  k $\Omega$  cm and  $\sim 0.33$  nF cm<sup>-1</sup>, respectively. The low-frequency data in Fig. 2(a) show the presence of a large arc (or arcs) that cannot be analyzed at  $300$  K but with  $R > 1$  M $\Omega$  cm. This electrical heterogeneity is most easily shown in the corresponding combined  $Z''$  and  $M''$  spectra at  $300$  K, which shows a large incline (but no peak) at high frequencies in the  $M''$  spectrum indicating the presence of a low-capacitance semiconducting component and a large incline (but no peak) at low frequencies in the  $Z''$  spectrum indicating the presence of a dominant insulating (and high-capacitance) component [Fig. 2(b)]. Subambient and higher-temperature measurements are therefore required to analyze the semiconducting and insulating components in more detail, respectively.

The high-frequency, nonzero intercept on the  $Z'$  axis of the  $Z^*$  plots developed into a poorly resolved arc at lower temperatures and therefore allowed both  $R$  and  $C$  values to be established for this semiconducting component. For example, the  $Z^*$  plot at  $148$  K with  $R \sim 10$  M $\Omega$  cm and  $C \sim 8$  pF cm<sup>-1</sup> as shown in Fig. 3(a). The magnitude of this capacitance is

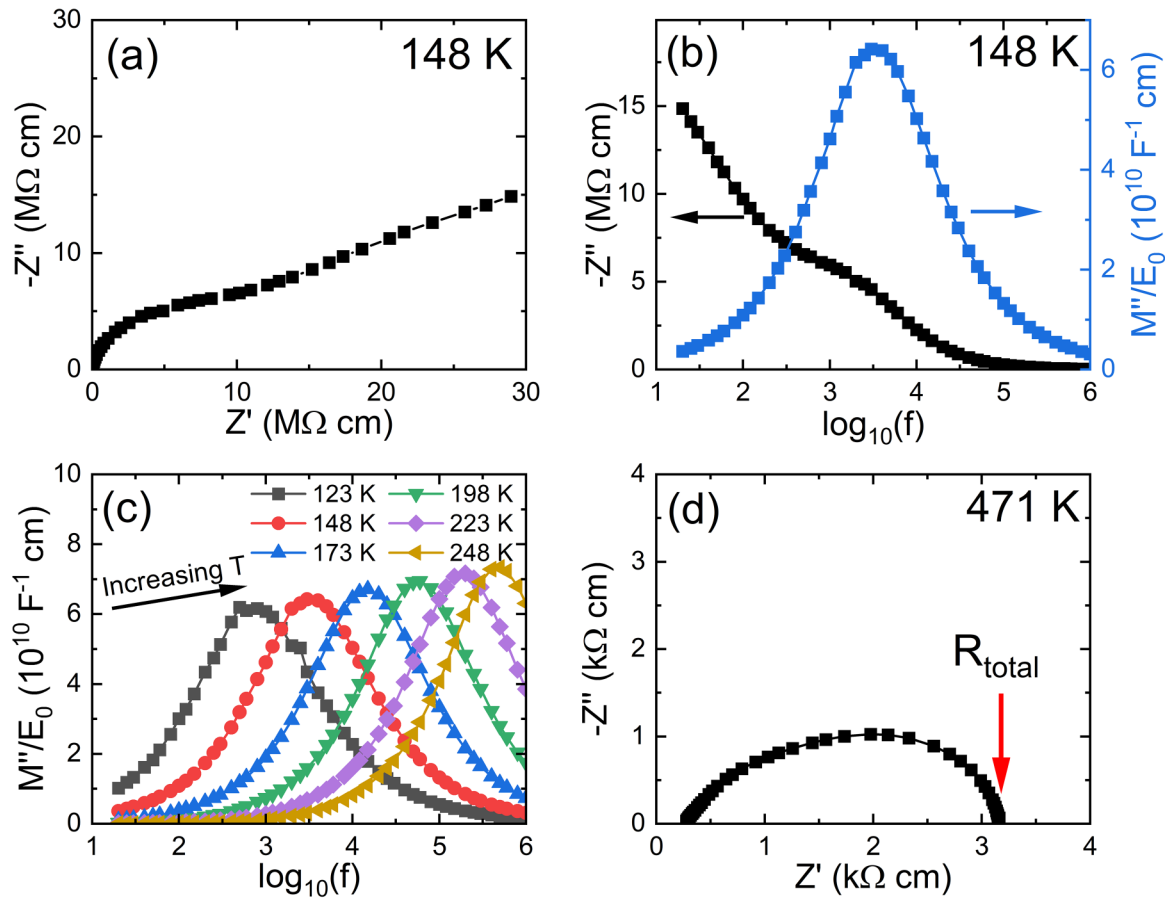


FIG. 3. (a)  $Z^*$  plot and (b)  $Z''$  and  $M''$  spectra for FeTiNbO<sub>6</sub> ceramics at 148 K. (c)  $M''$  spectra in temperature range 123 to 248 K and (d)  $Z^*$  plot at 471 K for FeTiNbO<sub>6</sub> ceramics.

consistent with a grain (or bulk) component and corresponds to a relative permittivity of  $\sim 90$ . Further confirmation of this semiconducting grain response is obtained from the corresponding  $Z''$  and  $M''$  spectra that show evidence of a broad  $M''$  Debye-type peak [Fig. 3(b)]. This broadened  $M''$  peak highlights heterogeneity within the grain response and the  $Z''$  spectrum illustrates the impedance to be dominated by a component(s) at lower frequency other than the bulk. Due to the level of electrical heterogeneity evident in the IS data we have not performed detailed equivalent-circuit analysis using constant-phase elements on these data. For simplicity we have used this broadened Debye-like peak in the subambient  $M''$  spectra to identify and estimate the  $R_b$  and  $C_b$  values of the semiconducting grain (bulk) response of FeTiNbO<sub>6</sub> ceramics [Fig. 3(c)]. Due to the inverse relationship between the  $M''_{\max}$  peak height and capacitance, the weak increase in the  $M''$  peak height with increasing temperature indicates  $C_b$  decreases with increasing temperature. An Arrhenius plot of the grain conductivity ( $\sigma_b = 1/R_b$ ) and the temperature dependence of the relative permittivity  $\epsilon_r = C_b/\epsilon_0$ , are shown in Fig. 4. This highlights FeTiNbO<sub>6</sub> ceramics to have semiconducting grains with a bulk activation energy for conduction of  $\sim 0.16$  eV [Fig. 4(a)], and weak temperature-dependent permittivity that is similar in magnitude and temperature dependence to undoped TiO<sub>2</sub> as shown in Fig. 4(b).

To test for the influence of nonohmic contacts and/or surface-layer effects on the impedance response, the Au paste

electrodes were removed by polishing and replaced by InGa alloy on the same ceramic. This produced a dramatic change in the RT IS response as shown in Fig. 5. The  $Z^*$  plot for the InGa electrodes showed dramatic reductions (if not complete removal) of both the intermediate and low-frequency arcs that give rise to the high sample impedance with Au electrodes. The total resistance of the sample/InGa electrode system is now  $\sim 13$  kΩ cm as opposed to  $>1$  MΩ cm, which corresponds closely to the  $\sim 10$  kΩ cm nonzero intercept on the  $Z'$  axis that was estimated for the sample with Au contacts and attributed to the bulk (grain) response. This suggests that the intermediate and low-frequency arcs in  $Z^*$  plots at RT for Au electrodes [Fig. 2(a)], are predominantly associated with surface layer(s) and nonohmic contacts, respectively. Furthermore, the corresponding  $\epsilon'$ ,  $\epsilon''$ , and  $\tan \delta$  spectra show significant deviations below 100 kHz [Figs. 5(b) and 5(c)], respectively. For example, at 1 kHz,  $\epsilon'$  for the Au electrode sample exceeds that of InGa by at least one order of magnitude, whereas the corresponding  $\epsilon''$  data show a decrease of one order of magnitude [Fig. 5(b)]. As a consequence,  $\tan \delta$  at 1 kHz for the Au electrode sample is approximately two orders of magnitude lower with a value of  $\sim 0.8$  as opposed to  $\sim 80$  [Fig. 5(c)].

Given the level of electrical heterogeneity and the strong influence of electrode contacts, we have not attempted to use equivalent-circuit analysis on the lower-frequency arcs that are observed in the  $Z^*$  data at or above 300 K. Instead, we



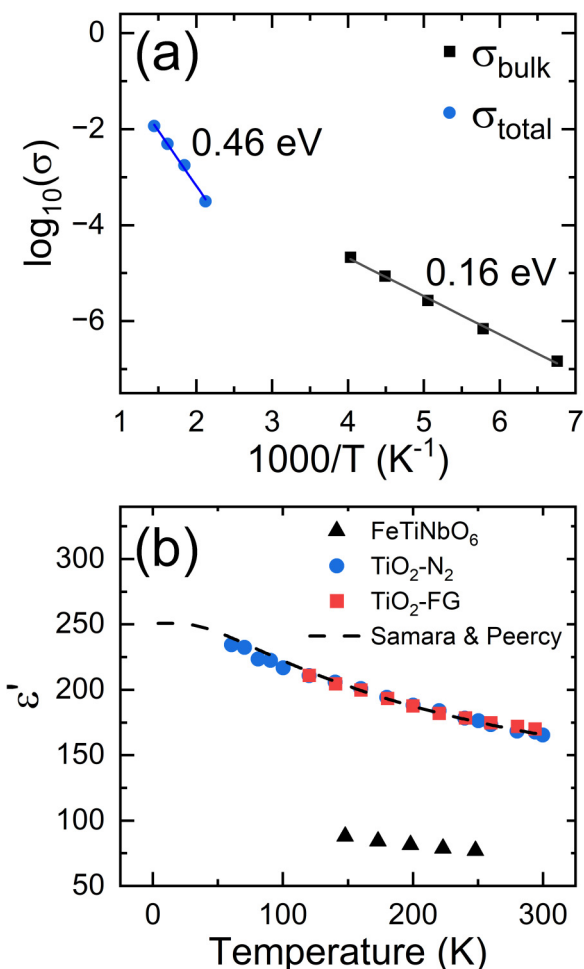


FIG. 4. (a) Arrhenius plot of bulk and total conductivity and (b) temperature dependence of bulk capacitance for FeTiNbO<sub>6</sub> ceramics. Data in (b) for undoped TiO<sub>2</sub> ceramics adapted from Ref. [5].

have analyzed the low-frequency intercept on the  $Z'$  axis in  $Z^*$  plots above 300 K for ceramics with Au contacts and taken this to correspond to the total (DC) resistivity of the ceramics. For example, a  $Z^*$  plot for data collected at 471 K shows this intercept to be  $\sim 3160 \Omega \text{ cm}$  [Fig. 3(d)]. An Arrhenius plot of the total conductivity ( $\sigma_T = 1/R_{DC}$ ) is shown in Fig. 4(a) and has an activation energy of  $\sim 0.46 \text{ eV}$ .

This preliminary study reveals the usefulness of combining DS and IS results (including subambient measurements and different electrode materials) to identify the origins of the apparent high-temperature RFE permittivity behavior in FeTiNbO<sub>6</sub> ceramics shown in Fig. 1(a) and as reported previously [11]. As opposed to being a bulk (intrinsic) phenomenon associated with nanoclustering of the cations [11], we propose it to be an extrinsic phenomenon that is primarily associated with nonohmic contacts (Schottky barriers) between semiconducting ceramics and Au electrodes. We suggest that low levels of nonstoichiometry associated with the acceptor-donor concentrations and potential mixed valency of both Fe and Ti give rise to bulk semiconductivity in these rutile-based ceramics but this requires more in-depth studies. This extrinsic effect dominates the DS and IS response, especially at and above RT. Decreasing the work function of the electrode

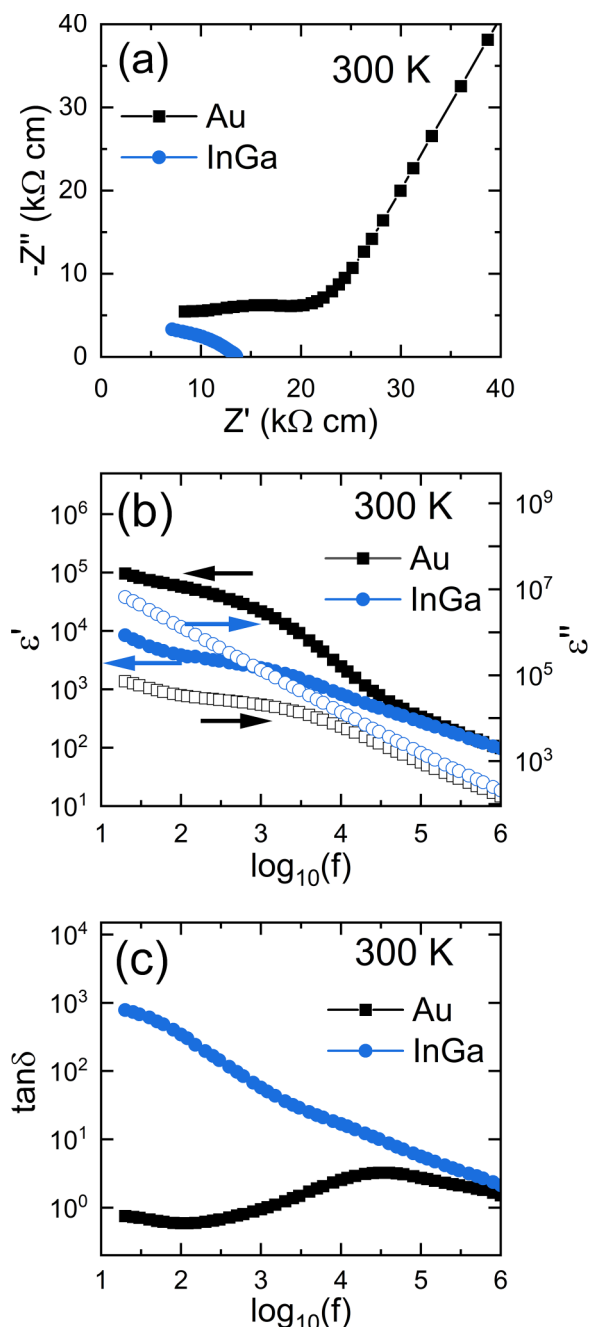


FIG. 5. (a)  $Z^*$  plots, (b)  $\epsilon'$  (filled symbols) and  $\epsilon''$  spectra and (c)  $\tan \delta$  vs frequency for FeTiNbO<sub>6</sub> ceramics with Au and InGa electrodes at room temperature.

material from  $\sim 5.3 \text{ eV}$  for Au [32] to  $\sim 4.1 \text{ eV}$  for InGa [33] is effective in reducing the contribution of nonohmic contacts (Schottky barriers) to the DS and IS response. This is similar to that observed in other materials reported to show CP behavior, i.e., single crystals and ceramics of CaCu<sub>3</sub>Ti<sub>4</sub>O<sub>12</sub> [26,27], which therefore suggests FeTiNbO<sub>6</sub> ceramics to be reduced and exhibit  $n$ -type behavior; however, further in-depth studies are required to fully assess this and other possible extrinsic contributions from surface layers and/or grain boundaries.

The DS results in Fig. 1 reveal multiple peaks in both permittivity and  $\tan \delta$  data over a wide temperature range

which suggests several relaxation mechanisms are involved. Based on the IS results, these are presumably linked to a combination of nonohmic contacts, surface and grain-boundary barrier-layer effects, and space-charge polarization (semiconductivity) similar to that reported for  $\text{CaCu}_3\text{Ti}_4\text{O}_{12}$  [26–28]. It is therefore important to establish the influence of the ceramic processing conditions (i.e., temperature-time- $p\text{O}_2$ ) on the source(s) and magnitude of the bulk semiconductivity and on both the physical and electrical microstructures. This is anticipated to be nontrivial given the possibility of: (i) coexisting mixed valent Ti and Fe ions in the ceramics; (ii) significant levels of oxygen nonstoichiometry (deficiency and/or excess) that can be induced in rutiles; (iii) segregation of the cations and/or oxygen concentration gradients at the grain boundaries and/or surfaces on the ceramics; and (iv) variations in grain size and porosity of ceramics. A substantial amount of further work is therefore required to elucidate the contributions of these various mechanisms to the electrical properties and DS of trirutile-based ceramics that contain acceptor-type transition metals such as Fe in  $\text{FeTiNbO}_6$  and  $\text{FeTiTaO}_6$ .

#### IV. CONCLUSIONS

Here, we present IS and DS data for  $\text{FeTiNbO}_6$  ceramics from  $\sim 10$  to 650 K, and a combination of  $Z^*$  plots and  $Z''$  and  $M''$  spectra are used to demonstrate the presence of electrical heterogeneity. Subambient  $M''$  spectra from 20 to  $10^6$  Hz demonstrate a semiconducting grain response with activation energy of  $\sim 0.16$  eV which develop Schottky barriers with Au electrodes, and a magnitude and temperature-dependent bulk permittivity comparable to undoped  $\text{TiO}_2$  ( $< 250$ ). Analyzing high-temperature  $Z^*$  plots and  $Z''$  spectra as well as changing the electrode material demonstrate that the large and temperature-dependent permittivity peak(s) ( $> 10^4$ ) observed at  $> 400$  K in the DS data are not an intrinsic phenomenon associated with cation nanoclustering to form polar nanodomains but rather a consequence of nonohmic contacts.

#### ACKNOWLEDGMENTS

We thank Dr. Jessica Andrews for collection of the SEM image shown in Fig. S2 and the Leverhulme Trust for financial support (Grant No. PRG-2020–007).

- 
- [1] A. Fujishima and K. Honda, Electrochemical photolysis of water at a semiconductor electrode, *Nature (London)* **238**, 37 (1972).
- [2] L. Nicolini, A new dielectric material, *Nature (London)* **170**, 938 (1952).
- [3] M. K. Nowotny, L. R. Sheppard, T. Bak, and J. Nowotny, Defect chemistry of titanium dioxide, *J. Phys. Chem. C* **112**, 5275 (2008).
- [4] B. O'Regan and M. Grätzel, A low-cost highefficiency solar cell based on dye-sensitized colloidal  $\text{TiO}_2$  films, *Nature (London)* **353**, 737 (1991).
- [5] J. Bonkerud, C. Zimmermann, P. M. Weiser, L. Vines, and E. V. Monakhov, On the permittivity of titanium dioxide, *Sci. Rep.* **11**, 12443 (2021).
- [6] R. A. Parker, Static dielectric constant of rutile ( $\text{TiO}_2$ ), 1.6–1060°K, *Phys. Rev.* **124**, 1719 (1961).
- [7] G. A. Samara and P. S. Peercy, Pressure and temperature dependence of the static dielectric constants and Raman spectra of  $\text{TiO}_2$  (rutile), *Phys. Rev. B* **7**, 1131 (1973).
- [8] J. H. Barrett, Dielectric constant in perovskite type crystals, *Phys. Rev.* **86**, 118 (1952).
- [9] W. H. Baur, The rutile type and its derivatives, *Crystallogr. Rev.* **13**, 65 (2007).
- [10] R. Mani, S. N. Achary, K. R. Chakraborty, S. K. Deshpande, J. E. Joy, A. Nag, J. Gopalakrishnan, and A. K. Tyagi,  $\text{FeTiTaO}_6$ : A lead-free relaxor ferroelectric based on the rutile structure, *Adv. Mater.* **20**, 1348 (2008).
- [11] R. Mani, S. N. Achary, K. R. Chakraborty, S. K. Deshpande, J. E. Joy, A. Nag, J. Gopalakrishnan, and A. K. Tyagi, Dielectric properties of some  $\text{MM}'\text{O}_4$  and  $\text{MTiM}'\text{O}_6$  ( $M = \text{Cr, Fe, Ga}$ ;  $M' = \text{Nb, Ta, Sb}$ ) rutile-type oxides, *J. Solid State Chem.* **183**, 1380 (2010).
- [12] Y. Shi, Y.-D. Hou, C. Wang, H.-Y. Ge, and M.-K. Zhu, Microstructure and relaxor behavior of dense fine-grain  $\text{FeTiTaO}_6$  ceramics, *J. Am. Ceram. Soc.* **93**, 2491 (2010).
- [13] R. A. Cowley, S. N. Gvasaliya, S. G. Lushnikov, B. Roessli, and G. M. Rotaru, Relaxing with relaxors: A review of relaxor ferroelectrics, *Adv. Phys.* **60**, 229 (2011).
- [14] L. E. Cross, Relaxor ferroelectrics, *Ferroelectrics* **76**, 241 (1987).
- [15] V. Bovtun, J. Petzelt, M. Kempa, D. Nuzhnyy, M. Savinov, S. Kamba, S. M. M. Yee, and D. A. Crandles, Wide range dielectric and infrared spectroscopy of (Nb + In) co-doped rutile ceramics, *Phys. Rev. Mater.* **2**, 075002 (2018).
- [16] D. A. Crandles, S. M. M. Yee, M. Savinov, D. Nuzhnyy, J. Petzelt, S. Kamba, and J. Prokeš, Electrode effects in dielectric spectroscopy measurements on (Nb + In) co-doped  $\text{TiO}_2$ , *J. Appl. Phys.* **119**, 154105 (2016).
- [17] W. Dong, W. Hu, A. Berlie, K. Lau, H. Chen, R. L. Withers, and Y. Liu, Colossal dielectric behavior of Ga + Nb co-doped rutile  $\text{TiO}_2$ , *ACS Appl. Mater. Interfaces* **7**, 25321 (2015).
- [18] W. Hu, Y. Liu, R. L. Withers, T. J. Frankcombe, L. Noren, A. Snashall, M. Kitchin, P. Smith, B. Gong, H. Chen *et al.*, Electron-pinned defect-dipoles for high-performance colossal permittivity materials, *Nat. Mater.* **12**, 821 (2013).
- [19] S. Kakimoto, Y. Hashimoto, T. Kuwano, K. Kimura, K. Hayashi, M. Hagiwara, K. Deguchi, and H. Taniguchi, Controlling dielectric properties of Nb + X ( $X = \text{Al, Ga, In}$ ) co-doped and Nb-doped rutile-type  $\text{TiO}_2$  single crystals, *J. Mater. Chem. C* **11**, 1304 (2023).
- [20] M. Kawarasaki, K. Tanabe, I. Terasaki, Y. Fujii, and H. Taniguchi, Intrinsic enhancement of dielectric permittivity in (Nb + In) co-doped  $\text{TiO}_2$  single crystals, *Sci. Rep.* **7**, 5351 (2017).
- [21] J. Li, F. Li, C. Li, G. Yang, Z. Xu, and S. Zhang, Evidences of grain boundary capacitance effect on the colossal dielectric permittivity in (Nb + In) co-doped  $\text{TiO}_2$  ceramics, *Sci. Rep.* **5**, 8295 (2015).

- [22] J. Li, F. Li, Y. Zhuang, L. Jin, L. Wang, X. Wei, Z. Xu, and S. Zhang, Microstructure and dielectric properties of (Nb + In) co-doped rutile TiO<sub>2</sub> ceramics, *J. Appl. Phys.* **116**, 074105 (2014).
- [23] Y. Song, X. Wang, Y. Sui, Z. Liu, Y. Zhang, H. Zhan, B. Song, Z. Liu, Z. Lv, L. Tao *et al.*, Origin of colossal dielectric permittivity of rutile Ti<sub>0.9</sub>In<sub>0.05</sub>Nb<sub>0.05</sub>O<sub>2</sub>: Single crystal and polycrystalline, *Sci. Rep.* **6**, 21478 (2016).
- [24] H. Taniguchi, D. Sato, A. Nakano, and I. Terasaki, Permittivity boosting in ‘yellow’ (Nb + In) co-doped rutile ceramics, *J. Mater. Chem. C* **8**, 13627 (2020).
- [25] Y. Q. Wu, X. Zhao, J. L. Zhang, W. B. Su, and J. Liu, Huge low-frequency dielectric response of (Nb,In)-doped TiO<sub>2</sub> ceramics, *Appl. Phys. Lett.* **107**, 242904 (2015).
- [26] M. C. Ferrarelli, D. C. Sinclair, A. R. West, H. A. Dabkowska, A. Dabkowski, and G. M. Luke, Comment on the origin(s) of the giant permittivity effect in CaCu<sub>3</sub>Ti<sub>4</sub>O<sub>12</sub> single crystals and ceramics, *J. Mater. Chem.* **19**, 5916 (2009).
- [27] M. Li, Z. Shen, M. Nygren, A. Feteira, D. C. Sinclair, and A. R. West, Origin(s) of the apparent high permittivity in CaCu<sub>3</sub>Ti<sub>4</sub>O<sub>12</sub> ceramics: Clarification on the contributions from internal barrier layer capacitor and sample-electrode contact effects, *J. Appl. Phys.* **106**, 104106 (2009).
- [28] D. C. Sinclair, T. B. Adams, F. D. Morrison, and A. R. West, CaCu<sub>3</sub>Ti<sub>4</sub>O<sub>12</sub>: One step internal barrier layer capacitor, *Appl. Phys. Lett.* **80**, 2153 (2002).
- [29] J. T. S. Irvine, D. C. Sinclair, and A. R. West, Electroceramics: Characterization by impedance spectroscopy, *Adv. Mater.* **2**, 132 (1990).
- [30] See Supplemental Material at <http://link.aps.org/supplemental/10.1103/PhysRevMaterials.7.114401> for Rietveld refinement data from x-ray diffraction, and a secondary electron image and grain-size distribution from scanning electron microscopy.
- [31] A. K. Jonscher, *Universal Relaxation Law* (Chelsea Dielectrics Press Ltd, London, 1996), Vol. 1, p. 196.
- [32] W. M. H. Sachtler, G. J. H. Dorgelo, and A. A. Holscher, The work function of gold, *Surf. Sci.* **5**, 221 (1966).
- [33] E. J. Lous, P. W. M. Blom, L. W. Molenkamp, and D. M. de Leeuw, Formation of a Schottky barrier between eutectic Ga,In and thiophene oligomers, *J. Appl. Phys.* **81**, 3537 (1997).